Earth Planet. Sci. Lett. 648 (2024) 119067

Contents lists available at ScienceDirect

Earth and Planetary Science Letters

journal homepage: www.elsevier.com/locate/epsl

Tracing hydrous eclogite melts in the source of sanukitoids

L.M. Spencer [a,*], C. Albert [a,b], H.M. Williams [c], O. Nebel [d,e], I.J. Parkinson [f], R.H. Smithies [g], H. Bruno [h], M. Fowler [i], H. Moreira [i,j], C.J. Lissenberg [a], M.-A. Millet [a]

[a] School of Earth and Environmental Sciences, Cardiff University, Park Place, Cardiff CF10 3AT, United Kingdom
[b] Bureau de Recherches Géologiques et Minières, 3 Avenue Claude Guillemin, 45060 Orléans, France
[c] Department of Earth Sciences, University of Cambridge, Downing Street, Cambridge CB2 3EQ, United Kingdom
[d] School of Earth, Atmosphere and Environment, Monash University, 9 Rainforest Walk, Clayton, VIC 3800, Australia
[e] GEOMAR Helmholtz Centre for Ocean Research Kiel, Wischhofstr. 1-3, D-24148 Kiel, Germany
[f] School of Earth Sciences, University of Bristol, Queens Road, Bristol BS8 1RJ, United Kingdom
[g] Geological Survey of Western Australia, Department of Mines, Industry Regulation and Safety, Mineral House, 100 Plain Street, East Perth, WA 6004, Australia
[h] Programa de Pós-Graduação, Faculdade de Geologia (FGEL) – TEKTOS. UERJ, Rio de Janeiro State University, Rua São Francisco Xavier 524, Maracanã, Rio de Janeiro, Brazil
[i] School of the Environment, Geography and Geosciences, University of Portsmouth, Burnaby Road, Portsmouth PO1 3QL, United Kingdom
[j] Géosciences Montpellier, Université de Montpellier, Place Eugène Bataillon, 34095 Montpellier, France

A R T I C L E I N F O

Keywords:
Sanukitoid
Titanium isotopes
Eclogite melting
Archean

A B S T R A C T

Sanukitoids are unique Archean and early Proterozoic igneous rocks. They contain high amounts of Mg, Ni and Cr, showing they are mantle-derived melts, while they are also enriched in Sr and Ba and have relatively high K contents, requiring the involvement of an incompatible element-enriched component likely derived from recycled crustal material. The appearance of sanukitoids in the geological record coincides with a shift in continental crust composition, and both events have been linked to a change in geodynamic processes on Earth. However, uncertainties remain about sanukitoid petrogenesis, in particular whether their mantle source was metasomatised by a metabasite-derived silicate melt or by an aqueous fluid. Titanium (Ti) stable isotopes can trace magmatic processes where silicate melts are in equilibrium with Fe-Ti oxides and amphibole but are insensitive to fluid-driven processes, making them a suitable tool to investigate not only the formation of sanukitoid magmas but also their subsequent evolution. Here we present Ti isotope data (δ^{49}Ti) for a series of Neoarchean sanukitoids from the Yilgarn Craton that continuously covers the full compositional range of sanukitoids. These are complemented by Mesoarchean sanukitoids and Paleoarchean "sanukitoid-like" rocks from the Pilbara Craton, and by Paleoproterozoic sanukitoids from the São Francisco Craton/Paleocontinent. In addition, we analysed Paleozoic high Ba-Sr granite suites from Scotland, which are proposed to be Phanerozoic sanukitoid analogues.

Evolved sanukitoids, which formed after Fe-Ti oxide saturation, show a more muted δ^{49}Ti increase during differentiation compared to currently analysed modern calc-alkaline suites. This difference is best explained by removal of significant proportions of Ti during sanukitoid differentiation by magmatic hornblende, which fractionates Ti isotopes less strongly than Fe-Ti oxides. Combined with early oxide saturation at high Mg#, this suggests that sanukitoid parental magmas had H_2O contents and fO_2 at least as high as modern arc magmas. Primitive (pre-oxide saturation) sanukitoids, however, have significantly higher δ^{49}Ti (0.11–0.20‰) than modern arc basalts, the depleted mantle and the bulk silicate Earth (BSE). Their elevated δ^{49}Ti values cannot be explained by aqueous fluids alone in their mantle source, and instead require the involvement of a hydrous eclogite melt component formed in equilibrium with residual rutile. We favour generation of this metasomatic melt by fluid-fluxed eclogite partial melting, demonstrating that both metabasite melts and aqueous fluids are important for sanukitoid formation. The Ti isotope compositions of Archean and Paleoproterozoic sanukitoids therefore favour formation of the sanukitoid mantle source by a subduction-like process at least ~2.7 Ga.

* Corresponding author.
E-mail address: spencerlm1@cardiff.ac.uk (L.M. Spencer).

https://doi.org/10.1016/j.epsl.2024.119067
Received 17 July 2024; Received in revised form 3 October 2024; Accepted 8 October 2024
Available online 15 October 2024

1. Introduction

The appearance of sanukitoid magmas in the geological record in the late Archean to early Proterozoic marks an important transition in Earth evolution. During this period the composition of continental crust-forming magmas changed from the sodic tonalites, trondhjemites and granodiorites (TTG suites) characteristic of Archean (4.0 to 2.5 Ga) cratons, to the potassic granites that have dominated upper continental crust ever since. This shift in composition is thought to reflect a change in geodynamic processes towards modern day plate tectonics, and as a result, sanukitoid occurrence has often been linked to the onset of subduction (e.g. Smithies and Champion, 2000) or a change in subduction style (e.g. Laurent et al., 2014; Martin et al., 2009).

Sanukitoids are also compositionally transitional between Archean TTG suites and post-Archean granites (Martin et al., 2009). On average they are moderately potassic, and are enriched in both compatible (e.g. Mg, Ni, Cr) and incompatible (e.g. Ba, Sr, light rare earth elements (LREE)) elements, which shows they formed by interaction between mantle peridotite and an incompatible element-enriched component likely derived from recycled crustal material (e.g. Shirey and Hanson, 1984; Stern et al., 1989). Similar to TTGs, they display highly fractionated rare earth element (REE) patterns, while also showing calc-alkaline differentiation trends similar to post-Archean granites (e.g. de Oliveira et al., 2009; Martin et al., 2009).

Our understanding of the link between sanukitoids and a potential global geodynamic transition is limited by uncertainties about their petrogenesis. In particular, the source and nature (i.e. melt or aqueous fluid) of the incompatible element-enriched component(s) in sanukitoid source regions are debated. A recycled, garnet-bearing metabasite (amphibolite or eclogite) derived source component is commonly inferred due to the similarity between sanukitoid and TTG REE compositions (e.g. Martin et al., 2005, 2009). Some studies favour a metabasite-derived silicate melt because of the elevated La/Yb, Nb/Y and Sr/Y of sanukitoids relative to most modern arc magmas (e.g. Martin et al., 2009; Smithies and Champion, 2000). Other studies argue instead for a metabasite-derived aqueous fluid because sanukitoids display strong depletions in fluid-immobile high field strength elements (HFSE, e.g. Ti, Nb, Ta) coupled with enrichments in fluid-mobile large ion lithophile elements (LILE, e.g. Sr, Ba) (e.g. Lobach-Zhuchenko et al., 2008; Stern et al., 1989). Sediment-derived melts/fluids (e.g. Halla, 2005), carbonatitic melts (e.g. Steenfelt et al., 2005) and alkaline melts (e.g. Heilimo et al., 2010) have additionally been proposed as incompatible element-enriched components.

A second uncertainty concerns the mechanisms and timing of interaction between the enriched component(s) and mantle peridotite. The generally favoured model is a two-stage process where mantle peridotite is first metasomatised by the incompatible element-enriched component and then undergoes partial melting to form sanukitoid parental magmas (e.g. Shirey and Hanson, 1984; Smithies and Champion, 2000). However, experimental petrology has shown that a one-stage process where TTG-like melts assimilate predominantly olivine from peridotite as they ascend through the mantle can also generate magmas with sanukitoid compositions (Rapp et al., 1999, 2010). Recently, it has been proposed that sanukitoid magmas can evolve from lamprophyric magmas by amphibole-dominated fractional crystallisation (Smithies et al., 2018, 2019), which is a variation on the two-stage model as calc-alkaline lamprophyres form by low- to moderate-degree partial melting of metasomatised mantle.

Titanium (Ti) stable isotopes are proving to be a valuable tracer of magmatic processes, and Fe-Ti oxide-melt and amphibole-melt equilibria in particular (e.g. Deng et al., 2019; Hoare et al., 2020, 2022; Johnson et al., 2019, 2023; Millet et al., 2016; Zhao et al., 2020). By contrast, Ti isotopes are insensitive to fluid-driven processes, because Ti is insoluble in aqueous fluids. These properties have already provided significant insights into the role mafic lithologies play in forming continental crust. Most notably, Zhang et al. (2023) and Hoare et al. (2023) showed that the Ti isotope compositions of Archean TTGs can be explained by partial melting of metabasites with Ti-bearing oxides and amphibole as residual phases, followed by fractional crystallisation. In modern settings, Klaver et al. (2024) demonstrated the occurrence of slab melting in subduction zones by tracing rutile as a residual phase.

Here we present the Ti stable isotope compositions of Archean and Paleoproterozoic sanukitoids as well as of Paleozoic sanukitoid analogues to test models of the formation and evolution of sanukitoids. We find that primitive sanukitoids have significantly heavier Ti isotope compositions than the depleted mantle, the bulk silicate Earth (BSE) and modern arc basalts, which cannot be explained by metasomatism of their mantle source via aqueous fluids alone. Instead, primitive sanukitoids require the involvement of a metabasite melt component enriched in heavy Ti isotopes, which likely formed by fluid-fluxed partial melting of eclogite, favouring formation of the sanukitoid mantle source by a subduction-like process.

2. Samples and methods

To investigate the Ti isotope systematics of sanukitoids we selected Archean and Paleoproterozoic sanukitoid suites covering a range of ages and locations – the ~2950 Ma high-Mg diorite suite from the Pilbara Craton (Smithies and Champion, 2000), the ~2670 Ma Black Flag Group (BFG) from the Yilgarn Craton (Smithies et al., 2019, 2022), and the 2130±2 Ma Alto Maranhão suite (Moreira et al., 2018) and two ~2115 Ma sanukitoids (Bruno et al., 2021) from the São Francisco Craton and Paleocontinent respectively. Trace element modelling demonstrates that these suites primarily evolved via fractional crystallisation of hornblende-dominated assemblages (Seixas et al., 2013; Smithies et al., 2019). The Black Flag Group is unique among sanukitoid occurrences as it continuously covers a wide SiO_2 range (44–73 wt%), including primitive sanukitoids and calc-alkaline lamprophyres as well as the granitoids that evolved from them (Smithies et al., 2018, 2019). This characteristic makes the BFG perfectly suited for investigating both the formation of primitive sanukitoid magmas and their differentiation. The BFG has been divided into three geochemical subgroups – high La/Th (high Ni), high La/Th (low Ni) and low La/Th. The high La/Th subgroups have more radiogenic Nd isotope compositions and younger Nd model ages (T_{2DM}) than the low La/Th subgroup, suggesting the high La/Th subgroups had a younger and slightly more incompatible trace element-enriched mantle source than the low La/Th subgroup (Smithies et al., 2022). We also analysed three ~3421 Ma samples from the Pilbara Craton which can be considered "sanukitoid-like rocks" because they share many geochemical characteristics with sanukitoids (e.g. high Ba and Sr concentrations, moderately potassic) but have lower Mg# (= 100*Mg/(Mg + Fe^{2+})), Ni and Cr and slightly shallower chondrite-normalised REE patterns than typical sanukitoids (Smithies et al., 2021; Vandenburg et al., 2023). Additionally, we looked at the ~425 Ma high Ba-Sr granite suites, including appinites, from Scotland which based on their petrology and geochemical composition are proposed to be Phanerozoic sanukitoid analogues (Fowler and Rollinson, 2012). These are late- to post-collisional magmas that formed during the Caledonian Orogeny, and it is proposed that their formation was triggered by slab breakoff (Fowler et al., 2008). Samples are from the Rogart and Strontian plutons, which are geochemically similar except the Rogart pluton displays enriched Sr and Nd isotope compositions, while the Strontian samples display Sr-Nd isotope compositions closer to depleted mantle values. This difference suggests that the Rogart mantle source was more contaminated by subducted sediment (Fowler et al., 2008). Detailed descriptions of the characteristics and geological context of each sample suite are provided in the supplementary material.

Mass-dependent Ti stable isotope compositions are expressed in delta notation relative to the Origins Laboratory Ti reference standard (OL-Ti) as $\delta^{49}Ti$, where $\delta^{49}Ti\ (‰) = 10^3[(^{49}Ti/^{47}Ti)_{sample}/(^{49}Ti/^{47}Ti)_{OL\text{-}Ti} - 1]$. A ^{47}Ti-^{49}Ti double spike was added to the samples before Ti purification using an established cation exchange chromatography method (Millet

and Dauphas, 2014; Zhang et al., 2011). Ti isotope compositions were measured using the Nu-Plasma II multicollector inductively coupled plasma mass spectrometer (MC-ICP-MS) at the Cardiff Earth Laboratory for Trace Element and Isotope Chemistry (CELTIC) at Cardiff University. To account for possible small polyatomic interferences on ^{47}Ti, all sample analyses were bracketed by measurements of the OL-Ti standard, while Ca interferences were monitored at mass 44. Uncertainties on the measurements are given as 95% confidence intervals (c.i.). A detailed description of the methodology is provided in the supplementary material. Reference materials BCR2, JB2 and RGM2 were prepared and analysed alongside each sample batch. The δ^{49}Ti of the reference materials measured here (BCR2 = -0.012±0.014‰, n = 2; JB2 = -0.014 ±0.018‰, n = 5; RGM2 = 0.580±0.019 ‰, n = 6) are in agreement with previous studies (e.g. Deng et al., 2019; Hoare et al., 2020; Millet et al., 2016; Zhao et al., 2020). All Ti isotope data are presented in supplementary dataset 1 (Spencer et al., 2024; https://doi.org/10.5880/digis.2024.004) alongside previously published major and trace element compositions of the samples.

3. Results

The δ^{49}Ti values of Archean and Paleoproterozoic sanukitoid samples vary from 0.108±0.023‰ to 0.291±0.021‰. The relatively primitive samples (SiO_2<58 wt%, MgO>5.5 wt%) precede oxide saturation; hence, they cover a more limited range (0.108–0.197‰) and their δ^{49}Ti is not correlated with indices of differentiation (Fig.1). These values are significantly higher than estimates of the δ^{49}Ti of the BSE (0.053 ±0.005‰, 2se; Deng et al., 2023) and depleted MORB (mid-ocean ridge basalt) mantle (DMM) (0.001±0.015‰, 2sd; Klaver et al., 2024). At SiO_2>58 wt% (i.e., after oxide saturation) δ^{49}Ti positively covaries with SiO_2 content (Fig.1a), similar to the differentiation trends seen in modern magma suites (e.g. Deng et al., 2019; Hoare et al., 2020; Millet et al., 2016). The Yilgarn sanukitoids extend to higher SiO_2 contents (>70 wt%) and δ^{49}Ti values (0.291‰) than the Pilbara and São Francisco sanukitoids (67 wt% and ~0.23‰, respectively).

The ~3.42 Ga sanukitoid-like rocks from the Pilbara Craton plot on the same δ^{49}Ti vs SiO_2 trend as the sanukitoids (Fig. 1a). These samples cover a limited compositional range at the upper end of this trend of 66.7 to 69.8 wt% SiO_2, and consequently have relatively high δ^{49}Ti values of 0.227±0.021‰ to 0.299±0.023‰. The Paleozoic high Ba-Sr

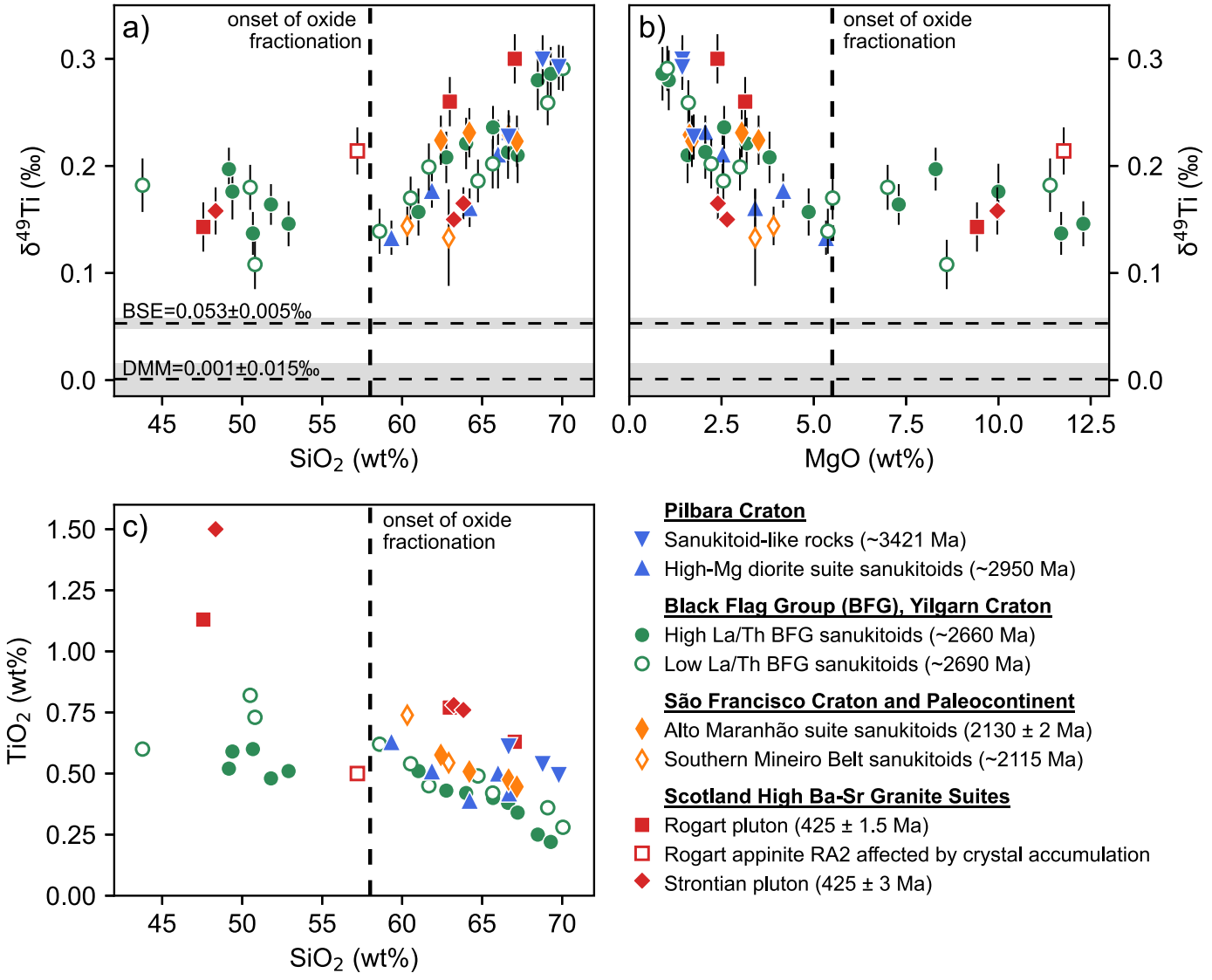

Fig. 1. a) δ^{49}Ti vs SiO_2, b) δ^{49}Ti vs MgO, and c) TiO_2 vs SiO_2 of Archean and Paleoproterozoic sanukitoids, Paleoarchean sanukitoid-like rocks and Paleozoic high Ba-Sr granites. Uncertainty in δ^{49}Ti is shown as the 95% confidence interval. BSE and DMM δ^{49}Ti values are from Deng et al. (2023) and Klaver et al. (2024) respectively, and the 2 standard error uncertainty is shown by the grey rectangles. The onset of oxide fractionation is determined from the inflection in the TiO_2 vs SiO_2 trend.

granite suites cover a similar δ^{49}Ti range to the Archean and Paleoproterozoic sanukitoids, varying between 0.143±0.023‰ and 0.300 ±0.023‰. Appinites from both the Rogart and Strontian plutons have indistinguishable δ^{49}Ti values of 0.143±0.023‰ and 0.158±0.022‰ respectively, similar to the more primitive sanukitoid samples.

4. Discussion

4.1. Effects of alteration, metamorphism and post-emplacement processes

The majority of Archean and Paleoproterozoic samples have experienced later metamorphism and/or alteration that may have affected their chemical and isotopic compositions (Bruno et al., 2021; Moreira et al., 2018; Smithies et al., 2004, 2019). Titanium is a HFSE with very low mobility in aqueous fluids (even at high salinity, see Rustioni et al., 2021) so protolith δ^{49}Ti values are expected to be largely unaffected by metamorphism and alteration involving aqueous fluids and brines. This is supported by the absence of correlation between δ^{49}Ti and LOI (loss on ignition), Ce anomaly (Ce/Ce*) and fluid mobile elements (e.g. Pb) in the samples studied here (supplementary fig. S1). Silicate melts, on the other hand, can transport significant amounts of Ti, and partial melting in the presence of residual Ti-bearing oxides can cause Ti isotope fractionation and produce melts with high δ^{49}Ti (e.g. Klaver et al., 2024). Two samples (MAJF 42 and 51B) from the São Francisco Paleocontinent have migmatitic textures showing they have undergone partial melting during metamorphism (Bruno et al., 2021). At comparable SiO_2 contents (60–63 wt%) these samples have δ^{49}Ti values nearly 0.1‰ lower than the unmigmatised Alto Maranhão suite from the nearby Mineiro Belt (Fig. 1a). However, these samples still broadly plot on the same overall trend as the other sanukitoids and their geochemical compositions show no obvious evidence of significant melt extraction, so we consider their Ti isotope compositions to be robust. The Paleozoic high Ba-Sr granite suites have not been affected by any later metamorphism (e.g. Fowler et al., 2008). The similarity of their Ti isotope compositions to those of the Archean and Paleoproterozoic sanukitoids therefore adds strength to the argument that δ^{49}Ti is not significantly affected by metamorphic processes.

Sample RA2 from the Rogart pluton has unusually high MgO and CaO for its SiO_2 content. This composition suggests that it has been affected by pyroxene-dominated crystal accumulation and may be significantly displaced from a true melt composition. No significant Ti isotope fractionation between pyroxene and silicate melt is expected (Leitzke et al., 2018; Rzehak et al., 2021; Wang et al., 2020), but RA2 shows slightly elevated δ^{49}Ti and may have been affected by accumulation of other minerals; hence, it is excluded from further discussion.

4.2. Differentiation of sanukitoids

While less evolved sanukitoids and appinites (<58 wt% SiO_2) show scattered but fairly constant δ^{49}Ti values between 0.1 and 0.2‰, the δ^{49}Ti values of the more evolved sanukitoids are correlated with indices of magma differentiation (SiO_2, MgO; Fig. 1), with the highest δ^{49}Ti measured in the most differentiated samples. The onset of this δ^{49}Ti increase coincides with TiO_2 content beginning to decrease (Fig. 1c). This observation supports the conclusion of previous studies that Ti isotope fractionation during magma differentiation is primarily caused by fractional crystallisation of Fe-Ti oxides such as titanomagnetite and ilmenite (e.g. Deng et al., 2019; Hoare et al., 2020; Millet et al., 2016).

Increasing δ^{49}Ti during differentiation has been observed in alkaline, tholeiitic and calc-alkaline magma series but the magnitude of this increase depends on the composition and abundance of Fe-Ti oxides, which themselves are a reflection of the TiO_2 concentration, water content and oxidation state of the magma (Aarons et al., 2020; Deng et al., 2023; Hoare et al., 2020, 2022; Johnson et al., 2023; Millet et al., 2016). Of these magma series, the calc-alkaline series shows the smallest increase in δ^{49}Ti during differentiation due to crystallisation of relatively small amounts of Ti-poor oxides and removal of significant proportions of Ti from the melt by silicates such as clinopyroxene, which do not significantly fractionate Ti isotopes (Hoare et al., 2020; Johnson et al., 2023). Sanukitoid magmas tend to follow a differentiation pathway akin to calc-alkaline magmas (e.g. de Oliveira et al., 2009; Martin et al., 2009). However, they display an even more muted δ^{49}Ti increase during differentiation than the modern calc-alkaline suites (Fig. 2a). This feature is also observed in the Paleoarchean sanukitoid-like rocks and Paleozoic high Ba-Sr granite suites (see supplementary material for a detailed discussion of the differentiation of the high Ba-Sr granite suites). We modelled the Ti isotope composition of evolving sanukitoid magmas using Rayleigh fractionation and the BFG sanukitoid suite, which is unique among sanukitoid occurrences as it covers a large and continuous range in SiO_2 content. The value of the bulk mineral-melt Ti isotope fractionation factor ($\alpha_{(solid\text{-}melt)}$) and the 2σ uncertainty were determined by weighted curve fitting to the measured δ^{49}Ti and calculated fraction of Ti remaining in the melt (F^{Ti}_{melt}) of the samples (a detailed description of the method used is provided in the supplementary material). The modelled $\alpha_{(solid\text{-}melt)}$ values for the BFG subgroups are distinctly higher than that of modern calc-alkaline suites at comparable SiO_2 contents (Hoare et al., 2020; Johnson et al., 2023) (Fig. 2b), thus indicating that the magnitude of Ti isotope fractionation during differentiation of sanukitoids is smaller than that of modern calc-alkaline magmas.

This difference is best explained by the fact that fractionating mineral assemblages in sanukitoids and their analogue suites are dominated by amphibole (Fowler et al., 2001; Seixas et al., 2013; Smithies et al., 2019; Smithies and Champion, 2000). This contrasts with the calc-alkaline differentiation suites for which Ti isotope data are available, which contain either no (Agung, Santorini) or "trace" amounts (Rindjani) of hornblende (Johnson et al., 2023). Up to ~2 wt% TiO_2 can be incorporated in octahedral sites in igneous hornblende (e.g. Makino and Tomita, 1989). It is therefore expected to have lower δ^{49}Ti than melt, as confirmed by Mandl (2019) who measured a $\Delta^{49}Ti_{(amphibole\text{-}melt)}$ of -0.210‰ at ~775 °C. Mass balance calculations by Greber et al. (2021) also support amphibole having lower δ^{49}Ti than melt, with $\Delta^{49}Ti_{(amphibole\text{-}melt)}$ of -0.30‰ at ~780 °C. Taken together, these results indicate that hornblende fractionates Ti isotopes more strongly than other Ti-bearing silicates such as clinopyroxene (Rzehak et al., 2021; Wang et al., 2020), but not as strongly as Fe-Ti oxides (e.g. Hoare et al., 2022). This implies that removal of a significant proportion of Ti by hornblende instead of oxides would reduce Ti isotope fractionation during differentiation and increase the bulk $\alpha_{(solid\text{-}melt)}$. Hornblende is proposed to be an early crystallising phase in the BFG (Smithies et al., 2018, 2019). The absence of clear correlation between δ^{49}Ti and SiO_2 or MgO contents in pre-oxide saturation (SiO_2<58 wt, MgO>5.5 wt%) samples (Figs. 1a and b) further suggests that hornblende fractional crystallisation did not cause significant Ti isotope fractionation in the BFG. We therefore propose that the more muted δ^{49}Ti increase seen during sanukitoid magma differentiation is due to removal of significant proportions of Ti by hornblende with limited associated isotope fractionation.

Hoare et al. (2020) found that δ^{49}Ti starts to increase at higher Mg# in more water-rich, oxidised arc magmas because these conditions promote earlier oxide saturation. As discussed earlier, this inflection in sanukitoid δ^{49}Ti marks the onset of Fe-Ti oxide crystallisation, so this relationship can provide insights into the water content and oxidation of sanukitoid parental magmas. Sanukitoid δ^{49}Ti starts to increase at high Mg# (~60–70), suggesting early oxide saturation relative to modern arc suites (Fig. 3). This implies that sanukitoid parental magmas had high water contents and oxygen fugacity (fO_2) comparable to modern arc magmas. This conclusion is in agreement with the findings of de Oliveira et al. (2010) and Nascimento et al. (2021, 2023) from mineral chemistry that sanukitoid parental magmas contained >7wt% H_2O and had fO_2 of NNO+0.3 to NNO+2.5 (log units relative to the nickel-nickel oxide buffer). High magma Ti and Fe contents may also drive earlier oxide

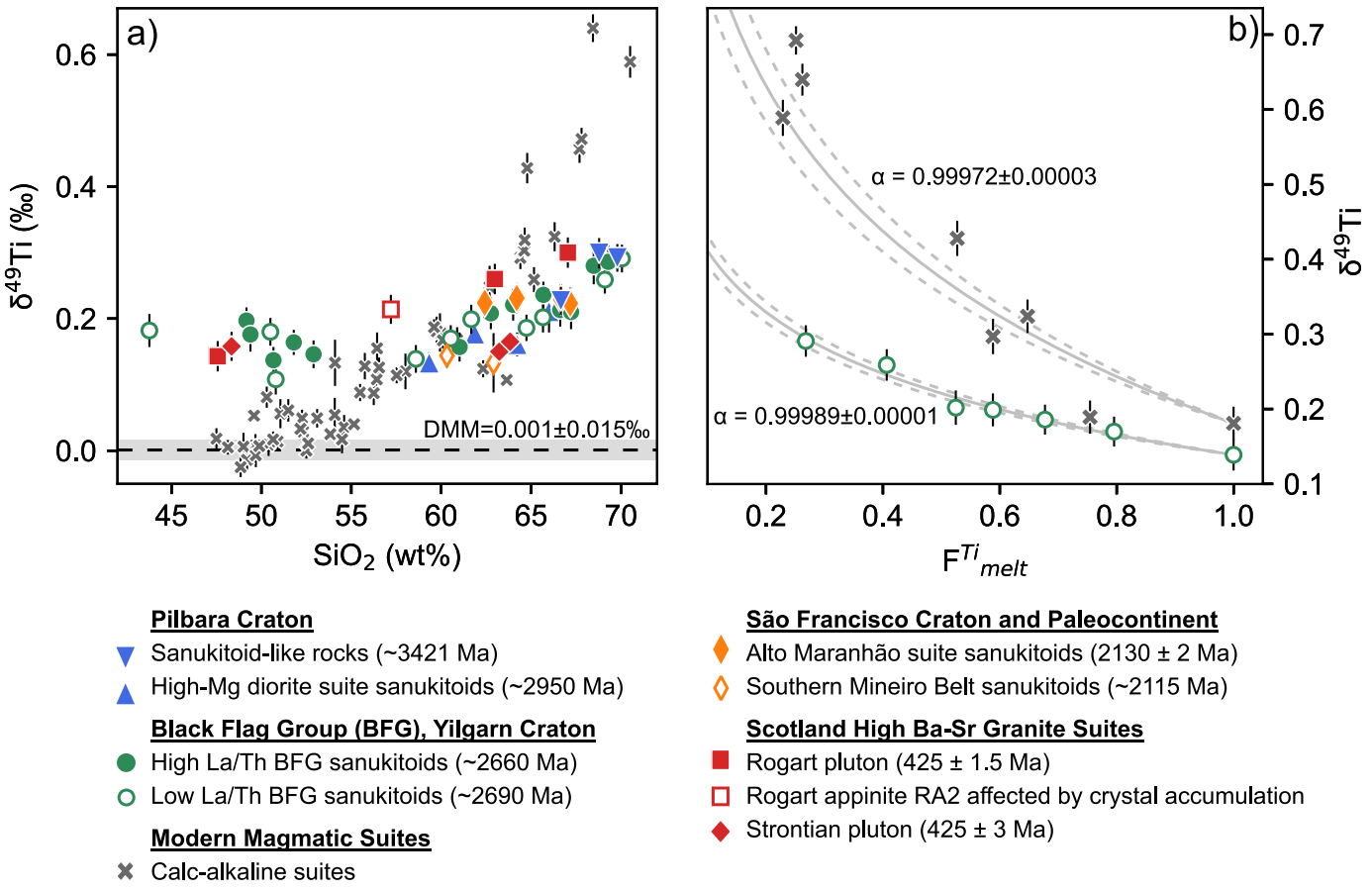

Fig. 2. Comparison between Archean and Paleoproterozoic sanukitoid suites and modern calc-alkaline suites. a) δ^{49}Ti vs SiO_2. Calc-alkaline suite data are from the New Britain arc (Millet and Dauphas, 2014), the Mariana arc (Millet et al., 2016), Agung volcano (Millet et al., 2016), the Tonga-Kermadec arc (Mandl et al., 2019), Santorini volcano (Hoare et al., 2020) and Rindjani Volcano (Johnson et al., 2023). DMM δ^{49}Ti value is from Deng et al. (2023) and the 2 standard error uncertainty is shown by the grey rectangle. b) δ^{49}Ti vs the fraction of Ti remaining in the melt (F^{Ti}_{melt}) for the low La/Th subgroup of the Black Flag Group sanukitoids and for Santorini. Rayleigh isotope fractionation models are shown in grey, with the dashed lines showing the 2σ uncertainty. Santorini δ^{49}Ti data and $\alpha_{(solid\text{-}melt)}$ are from Hoare et al. (2020).

saturation, but as the primitive sanukitoids here have low TiO_2 contents (<0.9 wt%) this is unlikely to be an important factor. Both early oxide fractionation and abundant hornblende crystallisation are consistent with sanukitoid parental magmas being water-rich and as such they require a H_2O-rich mantle source.

4.3. Formation of sanukitoid parental magmas

Sanukitoid and appinite samples with SiO_2<58 wt% and MgO>5.5 wt% display near constant, if slightly scattered, Ti isotope compositions. These samples precede Fe-Ti oxide saturation (Fig. 1) and their Ti isotope compositions were not affected by amphibole crystallisation. Their δ^{49}Ti values have therefore not been affected by fractional crystallisation and are likely representative of the Ti isotope composition of their parental melts. The δ^{49}Ti values of primitive sanukitoids range from 0.108±0.023‰ to 0.197±0.020‰. No Ti isotope fractionation is expected during partial melting of typical mantle lithologies (i.e. lherzolite, harzburgite) due to the absence of minerals such as Ti-bearing oxides (Millet et al., 2016), so melts would be expected to have δ^{49}Ti similar to the DMM (0.001±0.015‰, Klaver et al., 2024) or intermediate between the DMM and primordial mantle (0.053±0.005‰, Deng et al., 2023) for samples older than ~2.7 Ga. This is indeed the case for modern arc basalts, ocean island basalts (OIB), N- (normal-) MORB and Neoarchean komatiites (Fig. 4). However, primitive sanukitoids display significantly heavy Ti isotope compositions compared to ambient mantle and its melting products (Fig. 4). The mantle source of sanukitoids is widely considered to form by interaction between mantle peridotite and an incompatible element-enriched melt or aqueous fluid derived from recycled metabasite (e.g. Martin et al., 2009; Shirey and Hanson, 1984; Smithies and Champion, 2000; Stern et al., 1989). The high δ^{49}Ti of primitive sanukitoids indicates that the enriched component may therefore have had a heavy Ti isotope composition and/or that there was significant Ti isotope fractionation during partial melting of the putative metasomatised mantle source. Below, we use the Ti isotope data to test these competing models for sanukitoid formation.

4.3.1. Metabasite-derived aqueous fluids

As previously discussed, sanukitoid parental magmas were water-rich, requiring a H_2O-rich mantle source which may have been created through metasomatism of peridotite by aqueous fluids or silicate melts. We first investigate whether addition of metabasite-derived aqueous fluid alone to ambient mantle can explain the high δ^{49}Ti of primitive sanukitoids.

Titanium is a HFSE and is highly insoluble in aqueous fluids, even at high salinities (e.g. Rustioni et al., 2021). Hence, very little Ti is expected to be transferred from metabasites to fluids even in the presence of residual rutile, preventing fluids from being able impart a distinct high δ^{49}Ti signature to the sanukitoid source. The low Ti content of aqueous fluids also means that no rutile or other phases containing significant amounts of Ti are stabilised during partial melting of aqueous fluid-fluxed mantle (Till et al., 2012). Aqueous fluid-fluxed peridotite melts formed at 2950 – 2650 Ma should therefore have δ^{49}Ti

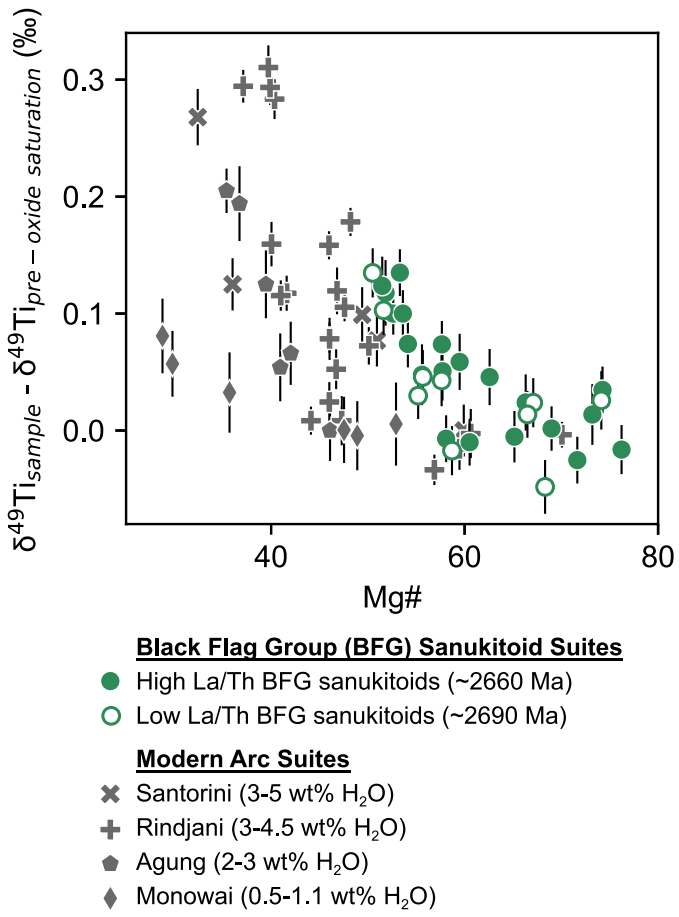

Fig. 3. $\delta^{49}Ti$ vs Mg# of the Black Flag Group sanukitoids and modern arc magmatic suites, based on figure 8 from Hoare et al. (2020). The y-axis is plotted as sample $\delta^{49}Ti$ minus the weighted mean $\delta^{49}Ti$ of pre-oxide saturations samples (where $\alpha_{(solid\text{-}melt)} \approx 1$) from that suite, to enable better comparison between suites. Modern arc magmatic suites are from Santorini volcano and Monowai seamount (Hoare et al., 2020), Rindjani Volcano (Johnson et al., 2023) and Agung Volcano (Millet et al., 2016).

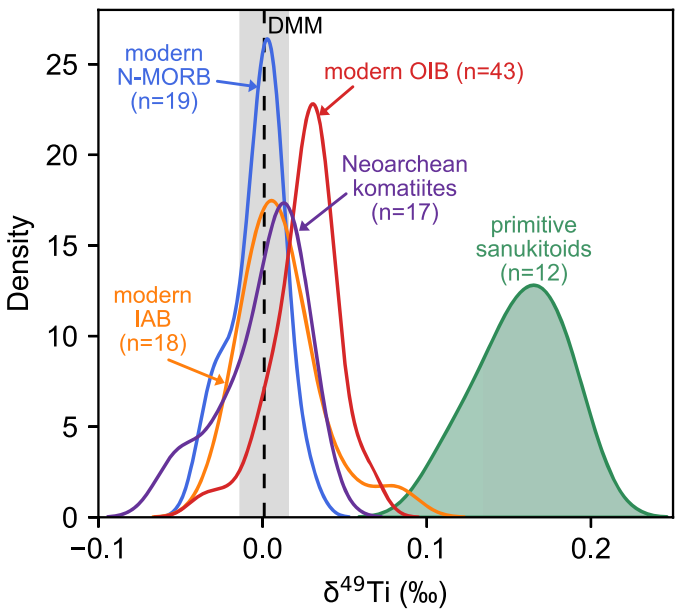

Fig. 4. Kernel density plots comparing the distribution of primitive (pre-oxide saturation) sanukitoid $\delta^{49}Ti$ to other primitive terrestrial magmas – modern N-MORB, ocean island basalts (OIB) and island arc basalts (IAB), and Neoarchean komatiites. Primitive terrestrial magma $\delta^{49}Ti$ data are from Deng et al. (2018, 2019, 2023), Greber et al. (2017); Hoare et al. (2020), Johnson et al. (2020, 2023), Millet & Dauphas (2014), Millet et al. (2016) and Zhao et al. (2020). DMM $\delta^{49}Ti$ value is from Klaver et al. (2024) and the 2 standard error uncertainty is shown by the grey rectangle.

indistinguishable from the late Archean ambient mantle (Fig. 5, Klaver et al., 2024), which we estimate from the weighted mean of Neoarchean komatiite $\delta^{49}Ti$ to be 0.001±0.003‰ (2se, $n = 17$) (Deng et al., 2023; Greber et al., 2017). This is not what is observed for the primitive sanukitoids, hence demonstrating that addition of aqueous fluids alone cannot explain their high $\delta^{49}Ti$ signature.

4.3.2. *Metabasite-derived partial melts*

Silicate melts have much higher Ti concentrations than aqueous fluids and hence have a greater capacity to impart a distinct Ti isotope signature onto the mantle. In eclogites Ti is mainly hosted in Ti-bearing oxides (predominantly rutile), and in amphibolites significant amounts of Ti can also be found in amphibole. Minor amounts of Ti can be present in pyroxenes and garnet but these minerals do not significantly fractionate Ti isotopes (Rzehak et al., 2021; Wang et al., 2020). During metabasite partial melting, light Ti isotopes are preferentially retained in 6-fold coordinated sites in residual rutile ± amphibole, generating melts with higher $\delta^{49}Ti$ than the protolith. This phenomenon has been invoked to explain the Ti isotope compositions of Archean TTG (Hoare et al., 2023; Zhang et al., 2023) and some modern primitive arc magmas (Klaver et al., 2024). It is therefore possible that a metabasite melt component could be responsible for the high $\delta^{49}Ti$ of primitive sanukitoids.

We further investigate this hypothesis by modelling partial melting of eclogite and amphibolite. Specifically, we calculate the Ti isotope composition of experimental partial melts (see Fig. 5 for references). $\Delta^{49}Ti_{melt\text{-}protolith}$ ($= \delta^{49}Ti_{melt} - \delta^{49}Ti_{protolith}$) was calculated using a mass balance approach following Klaver et al. (2021, 2024), and melt $\delta^{49}Ti$ was calculated using the average Neoarchean komatiite $\delta^{49}Ti$ (0.001 ±0.003‰) as the metabasite protolith composition (see supplementary material for full method). We modelled three different metabasite partial melting scenarios:

1. Anhydrous eclogite melting, where there is no H_2O in the system.
2. Dehydration melting, where aqueous fluid is formed by the breakdown of hydrous minerals within the metabasite – amphibole in amphibolite and phengite or zoisite in eclogite – creating water-undersaturated conditions during melting.
3. Fluid-fluxed melting, where externally derived aqueous fluid creates water-saturated conditions during melting.

The results of this modelling are presented in supplementary dataset 2 and Fig. 5.

Limited Ti isotope fractionation ($\delta^{49}Ti$ up to 0.051‰ at the smallest melt fractions) occurs during anhydrous eclogite melting, inconsistent with primitive sanukitoid data (Fig. 5). This limited fractionation is due to two main factors. First, high temperatures are required to cross the anhydrous solidus of eclogitic lithologies. For MORB-like compositions, this solidus lies between 1200 and 1350 °C at 2–5 GPa (e.g. Pertermann and Hirschmann, 2003; Spandler et al., 2008). Equilibrium stable isotope fractionation scales with $1/T^2$ so these high temperatures restrict the magnitude of Ti isotope fractionation (e.g. Young et al., 2015). Second, rutile is significantly more soluble in silicate melts at high temperatures (e.g. Gaetani et al., 2008). As a result, rutile rapidly disappears from the eclogitic residue, shifting the balance of the Ti budget towards the melt and thus muting any isotope fractionation. Any Ti still in the residue is now hosted by clinopyroxene and garnet, both of which are expected to have a weak preference for incorporating heavy Ti isotopes (Leitzke et al., 2018; Wang et al., 2020). This fractionation results in melts generated in the absence of residual rutile having slightly lower

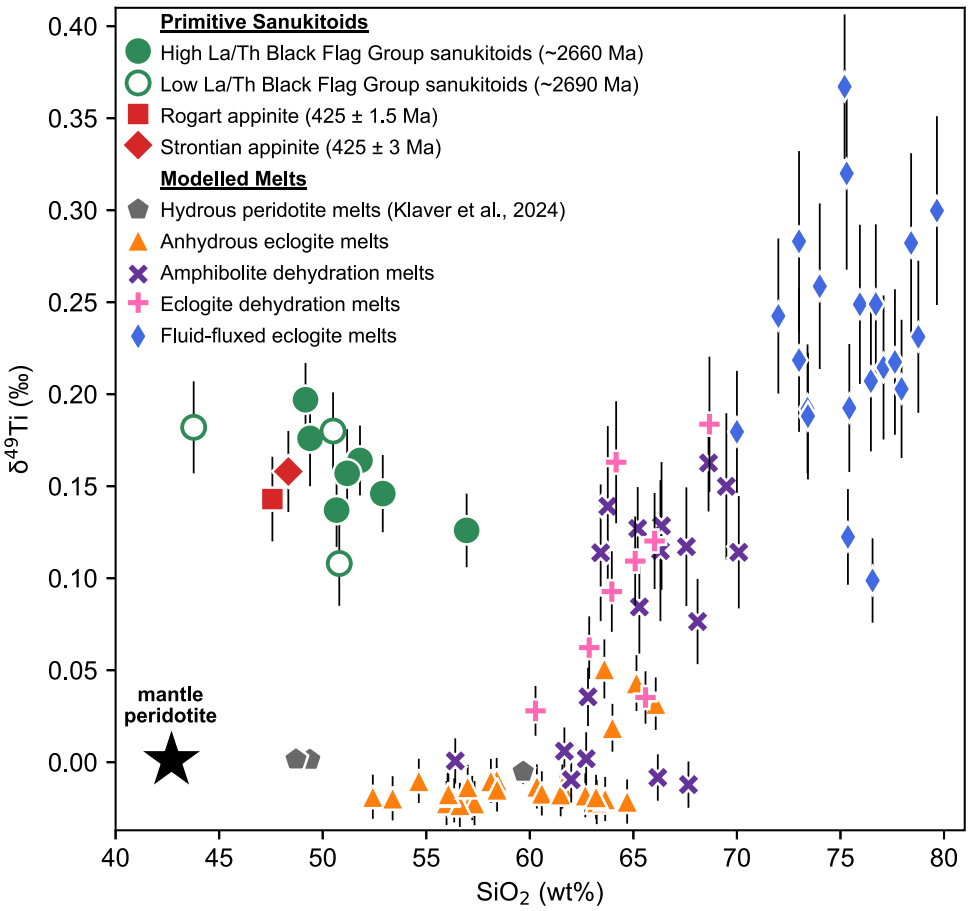

Fig. 5. δ^{49}Ti vs SiO_2 for primitive (pre-oxide saturation) Neoarchean sanukitoid samples and modelled partial melts of hydrous peridotite (Klaver et al., 2024) and metabasite. Uncertainty in measured sanukitoid δ^{49}Ti is shown as the 95% confidence interval. Uncertainty in modelled partial melt δ^{49}Ti is shown as the 2 s, calculated by linear uncertainty propagation. The black star is Neoarchean mantle peridotite, for which δ^{49}Ti is estimated from the weighted mean of Neoarchean komatiites (0.001±0.003‰, 2se, $n = 17$) (Deng et al., 2023; Greber et al., 2017). SiO_2 data for the modelled metabasite melts are from Carter et al. (2015), Kessel et al. (2005), Laurie and Stevens (2012), Martin & Hermann (2018), Massonne and Fockenberg (2022), Pertermann and Hirschmann (2003), Schmidt et al. (2004), Sen and Dunn (1994), Sisson and Kelemen (2018), Spandler et al. (2008), Wolf and Wyllie (1994), Yaxley and Green (1998) and Zhang et al. (2013).

δ^{49}Ti values than the metabasite protolith (Fig. 5).

The presence of aqueous fluids lowers metabasite solidus temperatures significantly and hence promotes rutile stability (e.g. Gaetani et al., 2008). Phengite-bearing eclogite dehydration melting begins at ~970 °C at 4 GPa (Massonne and Fockenberg, 2022), while zoisite-bearing eclogite dehydration occurs at <1025 °C (Skjerlie and Patiño Douce, 2002), meaning rutile remains stable at higher melt fractions during partial melting. Models of phengite-bearing eclogite dehydration melting show this results in melts with δ^{49}Ti values up to 0.184 ±0.035‰, higher than anhydrous eclogite melts, and generates melts with comparable δ^{49}Ti to the primitive sanukitoids (Fig. 5). Amphibolite dehydration melting, occurring at lower temperatures of 800–900 °C at 1–2 GPa (Sen and Dunn, 1994; Zhang et al., 2013), generates melts with somewhat lower δ^{49}Ti up to 0.163±0.023‰. The δ^{49}Ti of eclogite and amphibolite dehydration melts largely overlap (Fig. 5), despite the main residual minerals (rutile and amphibole respectively) hosting Ti being different. While rutile fractionates Ti isotopes more strongly than amphibole, eclogite dehydration melting occurs at higher temperatures than amphibolite dehydration melting, restricting the overall magnitude of Ti isotope fractionation. These model results imply that amphibolite and eclogite dehydration melts might be suitable metasomatic agents to explain the high δ^{49}Ti of primitive sanukitoids.

Fluid-fluxed eclogite melting under water-saturated conditions lowers the MORB-eclogite solidus even further to 750–800 °C at 2.2–4.5 GPa (e.g. Martin and Hermann, 2018; Schmidt et al., 2004; Sisson and Kelemen, 2018). The combination of abundant residual rutile and relatively low melting temperatures leads to significant Ti isotope fractionation with melt δ^{49}Ti between 0.099±0.020‰ and 0.367 ±0.037‰, depending on the temperature and proportion of rutile in the protolith. These values are largely similar to those calculated by Klaver et al. (2024) but extend to heavier melt δ^{49}Ti due to the inclusion of experiments with higher proportions of residual rutile from Laurie & Stevens (2012). These results show that fluid-fluxed eclogite melting can readily generate melts with δ^{49}Ti comparable to and higher than primitive sanukitoids (Fig. 5), and therefore mantle metasomatism by such melts would generate sanukitoid parental magmas enriched in heavy Ti isotopes.

Overall, the modelling demonstrates that the involvement of metabasite partial melt in the formation of sanukitoid parental magmas may be responsible for the heavy Ti isotope composition of primitive sanukitoids. However, the presence of aqueous fluid, either from the breakdown of hydrous minerals within metabasites or from an external source, is needed to generate melts with sufficiently high δ^{49}Ti.

4.3.3. *Ti isotope fractionation during interaction with mantle peridotite*

While significant Ti isotope fractionation occurs during metabasite melting, additional isotope fractionation may occur during interaction between the metabasite melts and mantle peridotite to form sanukitoid parental magmas. This interaction is generally thought to take place via a two-stage process where the mantle is metasomatised by metabasite melt and subsequently undergoes partial melting (e.g. Shirey and Hanson, 1984; Smithies and Champion, 2000), but a one-stage process

where the metabasite melt assimilates peridotite has also been proposed (Rapp et al., 1999, 2010). Experimental studies show that interaction between metabasite melt and peridotite generally consumes olivine and the melt, and forms orthopyroxene and (if temperatures are low enough) phlogopite and/or sodic amphibole (e.g. pargasite) (e.g. Gervasoni et al., 2017; Prouteau et al., 2001; Rapp et al., 1999, 2010; Sen and Dunn, 1994). These results are consistent with suggestions that the LILE enrichment in some sanukitoids requires a phlogopite ± amphibole-bearing source (Heilimo et al., 2010; Kovalenko et al., 2005; Lobach-Zhuchenko et al., 2008). No Ti-bearing accessory phases (e.g. oxides) were seen to form during the metabasite melt-peridotite reaction experiments, meaning that phlogopite and amphibole would be the main hosts of Ti in the sanukitoid mantle source. Pargasitic amphibole is the first phase to melt in this metasomatic assemblage, under both water-saturated and water-undersaturated conditions (Conceição and Green, 2004; Mengel and Green, 1989), so significant residual pargasite during sanukitoid parental magma genesis is unlikely. Phlogopite, on the other hand, is stable to higher temperatures and pressures than pargasite, particularly under water-saturated conditions when it can remain in the residue until >100 °C above the solidus (Conceição and Green, 2004). Multiple studies have proposed that a small amount of residual phlogopite during melting is needed to explain the LILE systematics of some sanukitoids, specifically their depletion in Rb alongside enrichment in Sr and Ba (Kovalenko et al., 2005; Laurent et al., 2011).

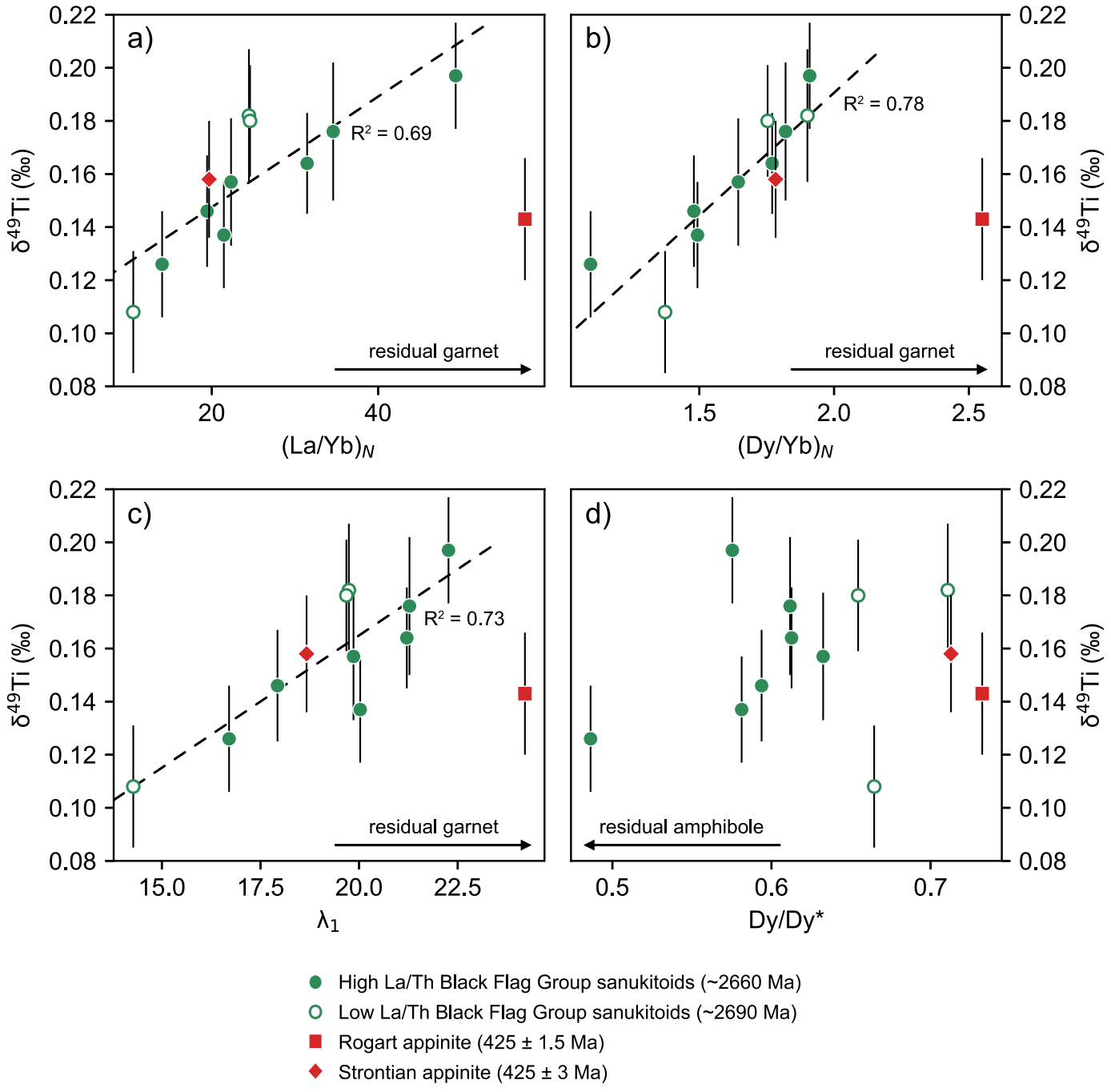

Fig. 6. Primitive sanukitoid and appinite δ^{49}Ti vs a) $(La/Yb)_N$, b) $(Dy/Yb)_N$, c) λ_1 (O'Neill, 2016) and d) Dy/Dy* (Davidson et al., 2013). The dashed lines are the least squares linear regressions of the Black Flag Group primitive sanukitoids and the Strontian appinite, with R^2 values for the regressions shown. REE concentrations are normalised to the CI chondrite values from O'Neill (2016).

Titanium is predominantly incorporated into octahedral M2 sites in phlogopite but substitution into 4-fold coordinated sites may also be possible in Ti-rich compositions (e.g. Bendeliani et al., 2023). Similar to amphibole, at equilibrium the difference in Ti coordination is expected to give phlogopite lower δ^{49}Ti than co-existing silicate melt, consistent with data on a biotite mineral separate from the Kneeling Nun Tuff, which yielded $\Delta^{49}Ti_{biotite\text{-}melt}$ = -0.234±0.060‰ at ~775 °C (Mandl, 2019). While $\Delta^{49}Ti_{phlogopite\text{-}melt}$ is poorly constrained, this suggests that Ti isotope fractionation may occur during partial melting of metasomatised mantle peridotite if residual phlogopite is present. Titanium isotope fractionation during partial melting of phlogopite-bearing peridotite was modelled based on experiments from Condamine et al. (2016) (see supplementary material for method and supplementary dataset 2 for results). Melts generated in equilibrium with small amounts (4–8 wt%) of residual phlogopite at 3 GPa and 1200–1300 °C are up to 0.047±0.012‰ (2sd) heavier than their metasomatised mantle protolith. While the melt compositions produced in these experiments are not analogous to parental sanukitoid magmas, these models demonstrate that the magnitude of Ti isotope fractionation due to residual phlogopite is small and will be limited by the low volume of phlogopite that can form from sodic metabasite melts (e.g. Prouteau et al., 2001). We therefore conclude that although small amounts of residual phlogopite in the sanukitoid mantle source can generate melts with higher δ^{49}Ti than their protolith, the magnitude of this fractionation is likely <0.05‰. Hence, we consider that formation of an isotopically heavy metabasite melt component in equilibrium with residual rutile ± amphibole is the main driver of high δ^{49}Ti in primitive sanukitoids.

4.3.4. Eclogite melts in the mantle source of sanukitoids

Both amphibolite and eclogite melts can match the Ti isotope fractionation observed in primitive sanukitoids. The δ^{49}Ti values of primitive sanukitoids, however, show strong positive covariation with tracers of garnet fractionation such as the CI-chondrite normalised REE ratios $(La/Yb)_N$ and $(Dy/Yb)_N$ (Fig. 6a and b). O'Neill (2016) demonstrated that polynomials can be fit to chondrite-normalised REE patterns to quantitatively describe their shape with shape coefficients (λ_n). λ_1 quantifies the steepness of REE patterns with higher values indicating a steeper slope. λ_1 is therefore a sensitive tracer of garnet fractionation, and positive covariation between λ_1 and δ^{49}Ti is also observed (Fig. 6c). No such covariation is seen with tracers of amphibole fractionation like $Dy/Dy^* = Dy_N/(La_N^{4/13} * Yb_N^{9/13})$, Fig. 6d) which is a measure of the relative middle rare earth element (MREE) depletion ($Dy/Dy^* < 1$) or enrichment ($Dy/Dy^* > 1$) of chondrite-normalised REE patterns (Davidson et al., 2013). The samples with the highest δ^{49}Ti and $(La/Yb)_N$ also have the lowest Yb concentrations (supplementary fig. S2), demonstrating that this signature is associated with heavy rare earth element (HREE) depletion and hence most likely caused by retention of HREEs in residual garnet. We note that the covariations are only perturbed by the single Rogart appinite sample displaying elevated $(La/Yb)_N$, $(Dy/Yb)_N$ and λ_1. Such a steep REE pattern is likely due to the significant recycled sediment input to the Rogart pluton mantle source (Fowler et al., 2008). This strong correlation therefore implies that the heavy Ti isotope composition and the garnet signature in primitive sanukitoids share a common origin. In contrast there is no clear evidence for a link between high δ^{49}Ti and residual amphibole, suggesting that amphibolite is not a suitable source for the metabasite melt component in sanukitoids. The combined Ti isotope and trace element compositions of primitive sanukitoids thus favour the metasomatic agent being an eclogite melt formed in equilibrium with residual rutile and garnet. Critically, the Ti isotope composition of primitive sanukitoids implies that eclogite partial melting occurred during the late Archean.

However, sanukitoids are not pure eclogite melts, but rather magmas originating from a mantle metasomatised by such melts (e.g. Martin et al., 2009; Shirey and Hanson, 1984). The high δ^{49}Ti signature of the eclogite melts will hence be diluted by interaction with low δ^{49}Ti mantle (0.001±0.003‰) and subsequent melting of the metasomatised source. It follows that the eclogite melt should have δ^{49}Ti significantly higher than the primitive sanukitoids: if not, and without significant additional Ti isotope fractionation due to residual phlogopite, the contribution of Ti from the mantle would have to be negligible for the high δ^{49}Ti signature of eclogite melts to be retained and transferred to the sanukitoid parental magmas. Sanukitoid major and trace element systematics rule out this scenario, with their high Mg# and Ni and Cr contents requiring a significant ultramafic peridotite component in their source (e.g. Martin et al., 2009). Hence, only eclogite melts with δ^{49}Ti significantly higher than the primitive sanukitoids can account for the data. Our modelling shows that dehydration melting of eclogite generates melts with δ^{49}Ti that overlaps with the sanukitoids, whereas fluid-fluxed eclogite melting results in melts with δ^{49}Ti exceeding that of the sanukitoids. We thus favour mantle peridotite metasomatised by fluid-fluxed eclogite melts as the likely origin of the heavy Ti isotope signature of primitive sanukitoids.

4.4. Geodynamic implications

Archean geodynamics are hotly debated and consequently multiple different geodynamic settings have been proposed for the formation of the sanukitoid mantle source (e.g. Bédard, 2006; Nebel et al., 2018; Stern et al., 1989). While geochemistry alone cannot pinpoint geodynamic setting, the results presented here provide new constraints on sanukitoid formation. The Ti stable isotope compositions of sanukitoids imply that they formed from water-rich, oxidised parental magmas that were likely generated from a mantle source metasomatised by fluid-fluxed eclogite partial melts. This result suggests that the mantle source of Archean and Paleoproterozoic sanukitoids must have formed in a geodynamic setting: 1) capable of recycling mafic rocks along low enough geothermal gradients (<~12 °C/km, e.g. Moyen, 2011) to high enough pressures (>~1.8 GPa or >~60 km depth, e.g. Chapman et al., 2019) to form eclogite; and 2) with a suitable external source of aqueous fluids to trigger fluid-fluxed melting.

On the present-day Earth, a Benioff-style subduction environment readily meets both these requirements. Numerous previous studies have proposed formation of the sanukitoid mantle source in a subduction setting (e.g. Martin et al., 2009; Smithies and Champion, 2000; Stern et al., 1989). Dehydration of abyssal serpentinites in the downgoing lithosphere is a source of voluminous aqueous fluid at subarc depths in modern subduction zones (Guillot and Hattori, 2013) and is proposed to trigger fluid-fluxed eclogite melting in modern arcs (e.g. Yogodzinski et al., 2017). We propose that the sanukitoid mantle source may have been formed by a similar process. The dynamics, and even the feasibility, of subduction in the late Archean are debated (e.g. van Hunen and Moyen, 2012), primarily because mantle potential temperatures may have been up to 150 °C higher than present (e.g. Ganne and Feng, 2017). Numerical models show this would have caused higher geotherms in subduction zones and likely more frequent slab breakoff (e.g. van Hunen and van den Berg, 2008), both of which are conducive to the conditions for serpentinite-derived fluid-fluxed eclogite melting (e.g. Klaver et al., 2024). The constraints placed by an eclogitic protolith allow for slightly higher subduction geotherms of <~12 °C/km than present day (typically 5–8 °C/km, e.g. Penniston-Dorland et al., 2015; Syracuse et al., 2010). As the mantle cooled during the Proterozoic and Phanerozoic, subduction geotherms decreased and subduction likely became more stable with less frequent slab breakoff (e.g. van Hunen and van den Berg, 2008), meaning conditions for fluid-fluxed eclogite melting in subduction zones may have become less common. This could explain why occurrences of sanukitoid magmatism became significantly rarer after the late Archean-early Proterozoic (Martin et al., 2009).

Alternatively, numerical models suggest that sinking crustal drips may have been capable of transporting hydrated, near-surface material to mantle depths along geothermal gradients <~12 °C/km (e.g. François et al., 2014; Sizova et al., 2015). Some models additionally favour a scenario where drips, triggered through lateral crustal movement and

flow, are diverted and become asymmetric, creating a geometry that mimics, or may even represent, incipient subduction (Nebel et al., 2018). It is possible that such settings could generate eclogite, with dehydration of adjacent serpentinised komatiite/basalt releasing aqueous fluids to trigger fluid-fluxed eclogite melting (Hartnady et al., 2022; Tamblyn et al., 2023). Interaction of these melts with mantle peridotite could then generate the metasomatised mantle source of sanukitoids (e.g. Nebel et al., 2018; Smithies et al., 2021). While crustal drips may provide an alternative setting to subduction for formation of the sanukitoid mantle source in the Archean, the viability of crustal drips (e.g. Korenaga, 2021) and their ability to transport hydrated, near-surface material to mantle depths (e.g. Roman and Arndt, 2020) are debated. If crustal drips were to only involve the lowermost crust (e.g. Johnson et al., 2014), which is likely to be largely anhydrous, it is difficult to reconcile with our results favouring fluid-fluxed eclogite melting due to the lack of an external source of aqueous fluids in this scenario. This is also the reason why we argue that our results are inconsistent with formation of the sanukitoid mantle source by delamination and then melting of dense lower crustal eclogites (e.g. Bédard, 2006).

Our results therefore support the occurrence of fluid-fluxed eclogite melting and the formation of sanukitoid mantle sources by subduction-like processes at least as far back as ~2.7 Ga (the age of the oldest primitive sanukitoids in our study). In fact, as sanukitoids most likely formed by a two-stage process, the formation of the sanukitoid mantle source predates the age of magma emplacement, implying fluid-fluxed eclogite melting occurred before ~2.7 Ga. A later event – such as lithospheric extension (e.g. Laurent et al., 2014; Smithies et al., 2019), slab breakoff (e.g. Heilimo et al., 2010) or lithospheric delamination (e.g. Kovalenko et al., 2005) – subsequently created a thermal anomaly and triggered melting of the metasomatised mantle to generate sanukitoid parental magmas. Furthermore, we note that the ~2950 Ma sanukitoids and ~3421 Ma sanukitoid-like rocks from the Pilbara Craton follow the same differentiation trend as the ~2670 Ma BFG sanukitoids. This observation may imply that they too formed by the same processes as the younger sanukitoids involving fluid-fluxed eclogite melting, but the lack of primitive samples prevents us from confidently extending our interpretations further back in the Archean. Nevertheless, our study clearly indicates that investigation of primitive sanukitoid and related magmas could prove useful for better understanding the geodynamic evolution of the Early Earth.

5. Conclusion

We present the Ti stable isotope compositions of late Archean-early Proterozoic sanukitoids and Paleozoic sanukitoid analogues. We use the δ^{49}Ti values of samples formed before and after Fe-Ti oxide saturation to investigate the formation of the sanukitoid mantle source and the differentiation of sanukitoid magmas respectively. Post-Fe-Ti oxide saturation, sanukitoid suites show a more muted δ^{49}Ti increase during differentiation than currently analysed modern calc-alkaline suites. We ascribe this to the removal of significant proportions of Ti by hornblende, which fractionates Ti isotopes less than Fe-Ti oxides (Greber et al., 2021; Mandl, 2019). Furthermore, the onset of this δ^{49}Ti increase occurs at high Mg# compared to modern arc suites. This observation shows there was early oxide saturation in sanukitoid magmas and suggests that sanukitoid parental magmas had water contents and fO_2 at least as high as modern arc magmas.

Primitive (pre-Fe-Ti oxide saturation) sanukitoid samples have higher δ^{49}Ti values (0.11–0.20‰) than modern arc basalts, the depleted mantle and the BSE, which cannot be explained by aqueous fluids alone. Instead, the high δ^{49}Ti values of primitive sanukitoids require the involvement of a hydrous eclogite melt component formed in equilibrium with residual rutile. We favour generation of this metasomatic melt by fluid-fluxed eclogite partial melting, showing that both metabasite melts and aqueous fluids are important for sanukitoid formation. The Ti isotope compositions of primitive sanukitoids thus favour formation of the sanukitoid mantle source by a subduction-like process at least 2.7 Ga. The evidence supporting a subduction-like setting at 2.7 Ga presented here gives further credence to models linking the widespread appearance of sanukitoids in the geological record to a global geodynamic transition.

CRediT authorship contribution statement

L.M. Spencer: Writing – original draft, Visualization, Investigation, Conceptualization. **C. Albert:** Writing – review & editing, Investigation. **H.M. Williams:** Writing – review & editing. **O. Nebel:** Writing – review & editing. **I.J. Parkinson:** Writing – review & editing. **R.H. Smithies:** Writing – review & editing, Resources, Conceptualization. **H. Bruno:** Writing – review & editing, Resources. **M. Fowler:** Writing – review & editing, Resources. **H. Moreira:** Writing – review & editing, Resources. **C.J. Lissenberg:** Writing – original draft, Conceptualization. **M.-A. Millet:** Writing – original draft, Investigation, Conceptualization.

Declaration of competing interest

The authors declare the following financial interests/personal relationships which may be considered as potential competing interests:

Laura Spencer and Marc-Alban Millet report financial support was provided by UK Research and Innovation Natural Environment Research Council. Laura Spencer reports financial support was provided by Geological Survey of Western Australia. If there are other authors, they declare that they have no known competing financial interests or personal relationships that could have appeared to influence the work reported in this paper.

Acknowledgements

Edward Inglis, Lindsey Owen, Lizan Abdullah, Sofiya Valkova and Imane Fahi are thanked for their support and assistance in the laboratory. Anthony Oldroyd is thanked for his assistance with preparing samples. This manuscript benefited from discussions with Martijn Klaver and Émilie Bruand. L.M. Spencer acknowledges financial support from a NERC GW4+ Doctoral Training Partnership studentship (NE/S007504/1) and the Geological Survey of Western Australia CASE studentship STU40714. M.-A. Millet acknowledges financial support from NERC project NIIICE (NE/R001332/1). R.H. Smithies publishes with the permission of the Executive Director of the Geological Survey of Western Australia. Comments made by two anonymous reviewers helped to improve this manuscript. Fang-Zhen Teng is thanked for editorial handling. This is Cardiff EARTH CRediT Contribution 34.

Supplementary materials

Supplementary material associated with this article can be found, in the online version, at doi:10.1016/j.epsl.2024.119067.

Data availability

Data are available through the DIGIS Geochemical Data Repository at https://doi.org/10.5880/digis.2024.004.

References

Aarons, S.M., Reimink, J.R., Greber, N.D., Heard, A.W., Zhang, Z., Dauphas, N., 2020. Titanium isotopes constrain a magmatic transition at the Hadean-Archean boundary in the Acasta Gneiss Complex. Sci. Adv. 6 (50), eabc9959. https://doi.org/10.1126/sciadv.abc9959.

Bédard, J.H., 2006. A catalytic delamination-driven model for coupled genesis of Archaean crust and sub-continental lithospheric mantle. Geochim. Cosmochim. Acta 70 (5), 1188–1214. https://doi.org/10.1016/j.gca.2005.11.008.

Bendeliani, A.A., Eremin, N.N., Bobrov, A.V., 2023. Mechanisms and conditions of Ti and Cr incorporation in mantle phlogopite: The results of atomistic simulation. Phys. Chem. Miner. 50 (1), 8. https://doi.org/10.1007/s00269-023-01232-x.

Bruno, H., Heilbron, M., de Morisson Valeriano, C., Strachan, R., Fowler, M., Bersan, S., Moreira, H., Motta, R., Almeida, J., Almeida, R., Carvalho, M., Storey, C., 2021. Evidence for a complex accretionary history preceding the amalgamation of Columbia: The Rhyacian Minas-Bahia Orogen, southern São Francisco Paleocontinent, Brazil. Gondwana Research 92, 149–171. https://doi.org/10.1016/j.gr.2020.12.019.

Carter, L.B., Skora, S., Blundy, J.D., De Hoog, J.C.M., Elliott, T., 2015. An Experimental Study of Trace Element Fluxes from Subducted Oceanic Crust. Journal of Petrology 56 (8), 1585–1606. https://doi.org/10.1093/petrology/egv046.

Chapman, T., Clarke, G.L., Daczko, N.R., 2019. The role of buoyancy in the fate of ultra-high-pressure eclogite. Sci. Rep. 9 (1), 19925. https://doi.org/10.1038/s41598-019-56475-y.

Conceição, R.V., Green, D.H., 2004. Derivation of potassic (shoshonitic) magmas by decompression melting of phlogopite+pargasite lherzolite. Lithos. 72 (3), 209–229. https://doi.org/10.1016/j.lithos.2003.09.003.

Condamine, P., Médard, E., Devidal, J.L., 2016. Experimental melting of phlogopite-peridotite in the garnet stability field. Contributions to Mineralogy and Petrology 171 (11), 95. https://doi.org/10.1007/s00410-016-1306-0.

Davidson, J., Turner, S., Plank, T., 2013. Dy/Dy*: Variations Arising from Mantle Sources and Petrogenetic Processes. Journal of Petrology 54 (3), 525–537. https://doi.org/10.1093/petrology/egs076.

de Oliveira, M.A., Dall'Agnol, R., Althoff, F.J., Leite, da Silva, A, A, 2009. Mesoarchean sanukitoid rocks of the Rio Maria Granite-Greenstone Terrane, Amazonian craton, Brazil. J. South. Am. Earth. Sci. 27 (2), 146–160. https://doi.org/10.1016/j.jsames.2008.07.003.

de Oliveira, M.A., Dall'Agnol, R., Scaillet, B, 2010. Petrological Constraints on Crystallization Conditions of Mesoarchean Sanukitoid Rocks, Southeastern Amazonian Craton, Brazil. Journal of Petrology 51 (10), 2121–2148. https://doi.org/10.1093/petrology/egq051.

Deng, Z., Chaussidon, M., Savage, P., Robert, F., Pik, R., Moynier, F., 2019. Titanium isotopes as a tracer for the plume or island arc affinity of felsic rocks. Proceedings of the National Academy of Sciences 116 (4), 1132–1135. https://doi.org/10.1073/pnas.1809164116.

Deng, Z., Moynier, F., Sossi, P.A., Chaussidon, M., 2018. Bridging the depleted MORB mantle and the continental crust using titanium isotopes. Geochem. Perspect. Lett. 11–15. https://doi.org/10.7185/geochemlet.1831.

Deng, Z., Schiller, M., Jackson, M.G., Millet, M.A., Pan, L., Nikolajsen, K., Saji, N.S., Huang, D., Bizzarro, M., 2023. Earth's evolving geodynamic regime recorded by titanium isotopes. Nature 621 (7977), 7977. https://doi.org/10.1038/s41586-023-06304-0. Article.

Fowler, M.B., Henney, P.J., Darbyshire, D.P.F., Greenwood, P.B., 2001. Petrogenesis of high Ba–Sr granites: The Rogart pluton, Sutherland. J. Geol. Soc. London. 158 (3), 521–534. https://doi.org/10.1144/jgs.158.3.521.

Fowler, M.B., Kocks, H., Darbyshire, D.P.F., Greenwood, P.B., 2008. Petrogenesis of high Ba–Sr plutons from the Northern Highlands Terrane of the British Caledonian Province. Lithos. 105 (1), 129–148. https://doi.org/10.1016/j.lithos.2008.03.003.

Fowler, M., Rollinson, H., 2012. Phanerozoic sanukitoids from Caledonian Scotland: Implications for Archean subduction. Geology. 40 (12), 1079–1082. https://doi.org/10.1130/G33371.1.

François, C., Philippot, P., Rey, P., Rubatto, D., 2014. Burial and exhumation during Archean sagduction in the East Pilbara Granite-Greenstone Terrane. Earth. Planet. Sci. Lett. 396, 235–251. https://doi.org/10.1016/j.epsl.2014.04.025.

Gaetani, G.A., Asimow, P.D., Stolper, E.M., 2008. A model for rutile saturation in silicate melts with applications to eclogite partial melting in subduction zones and mantle plumes. Earth. Planet. Sci. Lett. 272 (3), 720–729. https://doi.org/10.1016/j.epsl.2008.06.002.

Ganne, J., Feng, X., 2017. Primary magmas and mantle temperatures through time. Geochemistry, Geophysics, Geosystems 18 (3), 872–888. https://doi.org/10.1002/2016GC006787.

Gervasoni, F., Klemme, S., Rohrbach, A., Grützner, T., Berndt, J., 2017. Experimental constraints on mantle metasomatism caused by silicate and carbonate melts. Lithos. 282–283, 173–186. https://doi.org/10.1016/j.lithos.2017.03.004.

Greber, N.D., Dauphas, N., Bekker, A., Ptáček, M.P., Bindeman, I.N., Hofmann, A., 2017. Titanium isotopic evidence for felsic crust and plate tectonics 3.5 billion years ago. Science (1979) 357 (6357), 1271–1274. https://doi.org/10.1126/science.aan8086.

Greber, N.D., Pettke, T., Vilela, N., Lanari, P., Dauphas, N., 2021. Titanium isotopic compositions of bulk rocks and mineral separates from the Kos magmatic suite: Insights into fractional crystallization and magma mixing processes. Chemical Geology 578, 120303. https://doi.org/10.1016/j.chemgeo.2021.120303.

Guillot, S., Hattori, K., 2013. Serpentinites: Essential Roles in Geodynamics, Arc Volcanism, Sustainable Development, and the Origin of Life. Elements 9, 95–98. https://doi.org/10.2113/gselements.9.2.25.

Halla, J., 2005. Late Archean high-Mg granitoids (sanukitoids) in the southern Karelian domain, eastern Finland: Pb and Nd isotopic constraints on crust–mantle interactions. Lithos. 79 (1), 161–178. https://doi.org/10.1016/j.lithos.2004.05.007.

Hartnady, M.I.H., Johnson, T.E., Schorn, S., Hugh Smithies, R., Kirkland, C.L., Richardson, S.H., 2022. Fluid processes in the early Earth and the growth of continents. Earth. Planet. Sci. Lett. 594, 117695. https://doi.org/10.1016/j.epsl.2022.117695.

Heilimo, E., Halla, J., Hölttä, P., 2010. Discrimination and origin of the sanukitoid series: Geochemical constraints from the Neoarchean western Karelian Province (Finland). Lithos. 115 (1), 27–39. https://doi.org/10.1016/j.lithos.2009.11.001.

Hoare, L., Klaver, M., Muir, D.D., Klemme, S., Barling, J., Parkinson, I.J., Johan Lissenberg, C., Millet, M.A, 2022. Empirical and Experimental Constraints on Fe-Ti Oxide-Melt Titanium Isotope Fractionation Factors. Geochim. Cosmochim. Acta. https://doi.org/10.1016/j.gca.2022.02.011.

Hoare, L., Klaver, M., Saji, N.S., Gillies, J., Parkinson, I.J., Lissenberg, C.J., Millet, M.A., 2020. Melt chemistry and redox conditions control titanium isotope fractionation during magmatic differentiation. Geochim. Cosmochim. Acta 282, 38–54. https://doi.org/10.1016/j.gca.2020.05.015.

Hoare, L., Rzehak, L.J.A., Kommescher, S., Jansen, M., Rosing, M.T., Nagel, T., Millet, M.A., Hoffmann, J.E., Fonseca, R.O.C., 2023. Titanium isotope constraints on the mafic sources and geodynamic origins of Archean crust. Geochem. Perspect. Lett. 28, 1–6. https://doi.org/10.7185/geochemlet.2340.

Johnson, A.C., Aarons, S.M., Dauphas, N., Nie, N.X., Zeng, H., Helz, R.T., Romaniello, S.J., Anbar, A.D., 2019. Titanium isotopic fractionation in Kilauea Iki lava lake driven by oxide crystallization. Geochim. Cosmochim. Acta 264, 180–190. https://doi.org/10.1016/j.gca.2019.08.022.

Johnson, A.C., Zhang, Z.J., Dauphas, N., Rudnick, R.L., Foden, J.D., Toc, M., 2023. Redox and mineral controls on Fe and Ti isotopic fractionations during calc-alkaline magmatic differentiation. Geochim. Cosmochim. Acta 355, 1–12. https://doi.org/10.1016/j.gca.2023.06.016.

Johnson, T.E., Brown, M., Kaus, B.J.P., VanTongeren, J.A., 2014. Delamination and recycling of Archaean crust caused by gravitational instabilities. Nat. Geosci. 7 (1), 1. https://doi.org/10.1038/ngeo2019. Article.

Kessel, R., Ulmer, P., Pettke, T., Schmidt, M.W., Thompson, A.B., 2005. The water–basalt system at 4 to 6 GPa: Phase relations and second critical endpoint in a K-free eclogite at 700 to 1400°C. Earth. Planet. Sci. Lett. 237 (3), 873–892. https://doi.org/10.1016/j.epsl.2005.06.018.

Klaver, M., Luu, T.H., Lewis, J., Jansen, M.N., Anand, M., Schwieters, J., Elliott, T., 2021. The Ca isotope composition of mare basalts as a probe into the heterogeneous lunar mantle. Earth. Planet. Sci. Lett. 570, 117079. https://doi.org/10.1016/j.epsl.2021.117079.

Klaver, M., Yogodzinski, G., Albert, C., Camejo-Harry, M., Elburg, M., Hoernle, K., Macpherson, C., Nowell, G., Rushmer, T., Williams, H., Millet, M.A., 2024. Widespread slab melting in modern subduction zones. Earth. Planet. Sci. Lett. 626, 118544. https://doi.org/10.1016/j.epsl.2023.118544.

Korenaga, J., 2021. Hadean geodynamics and the nature of early continental crust. Precambrian. Res. 359, 106178. https://doi.org/10.1016/j.precamres.2021.106178.

Kovalenko, A., Clemens, J.D., Savatenkov, V., 2005. Petrogenetic constraints for the genesis of Archaean sanukitoid suites: Geochemistry and isotopic evidence from Karelia, Baltic Shield. Lithos. 79 (1), 147–160. https://doi.org/10.1016/j.lithos.2004.05.006.

Laurent, O., Martin, H., Doucelance, R., Moyen, J.F., Paquette, J.L., 2011. Geochemistry and petrogenesis of high-K "sanukitoids" from the Bulai pluton, Central Limpopo Belt, South Africa: Implications for geodynamic changes at the Archaean–Proterozoic boundary. Lithos. 123 (1), 73–91. https://doi.org/10.1016/j.lithos.2010.12.009.

Laurent, O., Martin, H., Moyen, J.F., Doucelance, R., 2014. The diversity and evolution of late-Archean granitoids: Evidence for the onset of "modern-style" plate tectonics between 3.0 and 2.5Ga. Lithos. 205, 208–235. https://doi.org/10.1016/j.lithos.2014.06.012.

Laurie, A., Stevens, G., 2012. Water-present eclogite melting to produce Earth's early felsic crust. Chemical Geology 314–317, 83–95. https://doi.org/10.1016/j.chemgeo.2012.05.001.

Leitzke, F.P., Fonseca, R.O.C., Göttlicher, J., Steininger, R., Jahn, S., Prescher, C., Lagos, M., 2018. Ti K-edge XANES study on the coordination number and oxidation state of Titanium in pyroxene, olivine, armalcolite, ilmenite, and silicate glass during mare basalt petrogenesis. Contributions to Mineralogy and Petrology 173 (12), 103. https://doi.org/10.1007/s00410-018-1533-7.

Lobach-Zhuchenko, S.B., Rollinson, H., Chekulaev, V.P., Savatenkov, V.M., Kovalenko, A.V., Martin, H., Guseva, N.S., Arestova, N.A., 2008. Petrology of a Late Archaean, Highly Potassic, Sanukitoid Pluton from the Baltic Shield: Insights into Late Archaean Mantle Metasomatism. Journal of Petrology 49 (3), 393–420. https://doi.org/10.1093/petrology/egm084.

Makino, K., Tomita, K., 1989. Cation distribution in the octahedral sites of hornblendes. American Mineralogist 74, 1097–1105.

Mandl, M.B., 2019. Titanium Isotope Fractionation On the Earth and Moon: Constraints on Magmatic Processes and Moon formation, p. 141. https://doi.org/10.3929/ETHZ-B-000351171 [ETH Zurich; Application/pdf].

Martin, H., Moyen, J.F., Rapp, R., 2009. The sanukitoid series: Magmatism at the Archaean–Proterozoic transition. Earth and Environmental Science Transactions of The Royal Society of Edinburgh 100 (1–2), 15–33. https://doi.org/10.1017/S1755691009016120.

Martin, H., Smithies, R.H., Rapp, R., Moyen, J.F., Champion, D., 2005. An overview of adakite, tonalite–trondhjemite–granodiorite (TTG), and sanukitoid: Relationships and some implications for crustal evolution. Lithos. 79 (1), 1–24. https://doi.org/10.1016/j.lithos.2004.04.048.

Martin, L.A.J., Hermann, J., 2018. Experimental Phase Relations in Altered Oceanic Crust: Implications for Carbon Recycling at Subduction Zones. Journal of Petrology 59 (2), 299–320. https://doi.org/10.1093/petrology/egy031.

Massonne, H.J., Fockenberg, T., 2022. Melting of phengite-bearing eclogite at pressures of 4 and 9 GPa relevant to deep regions of a subduction zone. Earth. Planet. Sci. Lett. 584, 117475. https://doi.org/10.1016/j.epsl.2022.117475.

Mengel, K., Green, D.H., 1989. Stability of amphibole and phlogopite in metasomatized peridotite under water-saturated and water-undersaturated conditions. Geological Society of Australia Special Publication No. 14 - Proceedings of the Fourth

International Kimberlite Conference, 1(Kimberlites and Related Rocks), pp. 571–581.
Millet, M.A., Dauphas, N., 2014. Ultra-precise titanium stable isotope measurements by double-spike high resolution MC-ICP-MS. J. Anal. At. Spectrom. 29 (8), 1444–1458. https://doi.org/10.1039/C4JA00096J.
Millet, M.A., Dauphas, N., Greber, N.D., Burton, K.W., Dale, C.W., Debret, B., Macpherson, C.G., Nowell, G.M., Williams, H.M., 2016. Titanium stable isotope investigation of magmatic processes on the Earth and Moon. Earth. Planet. Sci. Lett. 449, 197–205. https://doi.org/10.1016/j.epsl.2016.05.039.
Moreira, H., Seixas, L., Storey, C., Fowler, M., Lasalle, S., Stevenson, R., Lana, C., 2018. Evolution of Siderian juvenile crust to Rhyacian high Ba-Sr magmatism in the Mineiro Belt, southern São Francisco Craton. Geoscience Frontiers 9 (4), 977–995. https://doi.org/10.1016/j.gsf.2018.01.009.
Moyen, J.F., 2011. The composite Archaean grey gneisses: Petrological significance, and evidence for a non-unique tectonic setting for Archaean crustal growth. Lithos. 123 (1), 21–36. https://doi.org/10.1016/j.lithos.2010.09.015.
Nascimento, A.C.do, Oliveira, D.C.de, Gabriel, E.O., Marangoanha, B., Ribeiro da Silva, L., Aleixo, E.da C, 2023. Mineral chemistry of the Água Limpa suite: Insights into petrological constraints and magma ascent rate of Mesoarchean sanukitoids from the Sapucaia terrane (Carajás Province, southeastern Amazonian Craton, Brazil). J. South. Am. Earth. Sci. 132, 104683. https://doi.org/10.1016/j.jsames.2023.104683.
Nascimento, A.C.do, Oliveira, D.C.de, Silva, L.R.da, Lamarão, C.N, 2021. Mineral thermobarometry and its implications for petrological constraints on Mesoarchean granitoids from the Carajás Province, Amazonian Craton (Brazil). J. South. Am. Earth. Sci. 109, 103271. https://doi.org/10.1016/j.jsames.2021.103271.
Nebel, O., Capitanio, F.A., Moyen, J.F., Weinberg, R.F., Clos, F., Nebel-Jacobsen, Y.J., Cawood, P.A., 2018. When crust comes of age: On the chemical evolution of Archaean, felsic continental crust by crustal drip tectonics. Philosophical Transactions of the Royal Society A: Mathematical, Physical and Engineering Sciences 376 (2132), 20180103. https://doi.org/10.1098/rsta.2018.0103.
O'Neill, H.St.C, 2016. The Smoothness and Shapes of Chondrite-normalized Rare Earth Element Patterns in Basalts. Journal of Petrology 57 (8), 1463–1508. https://doi.org/10.1093/petrology/egw047.
Penniston-Dorland, S.C., Kohn, M.J., Manning, C.E., 2015. The global range of subduction zone thermal structures from exhumed blueschists and eclogites: Rocks are hotter than models. Earth. Planet. Sci. Lett. 428, 243–254. https://doi.org/10.1016/j.epsl.2015.07.031.
Pertermann, M., Hirschmann, M.M., 2003. Anhydrous Partial Melting Experiments on MORB-like Eclogite: Phase Relations, Phase Compositions and Mineral–Melt Partitioning of Major Elements at 2–3 GPa. Journal of Petrology 44 (12), 2173–2201. https://doi.org/10.1093/petrology/egg074.
Prouteau, G., Scaillet, B., Pichavant, M., Maury, R., 2001. Evidence for mantle metasomatism by hydrous silicic melts derived from subducted oceanic crust. Nature 410 (6825), 6825. https://doi.org/10.1038/35065583. Article.
Rapp, R.P., Norman, M.D., Laporte, D., Yaxley, G.M., Martin, H., Foley, S.F., 2010. Continent Formation in the Archean and Chemical Evolution of the Cratonic Lithosphere: Melt-Rock Reaction Experiments at 3-4 GPa and Petrogenesis of Archean Mg-Diorites (Sanukitoids). Journal of Petrology 51 (6), 1237–1266. https://doi.org/10.1093/petrology/egq017.
Rapp, R.P., Shimizu, N., Norman, M.D., Applegate, G.S., 1999. Reaction between slab-derived melts and peridotite in the mantle wedge: Experimental constraints at 3.8 GPa. Chemical Geology 160 (4), 335–356. https://doi.org/10.1016/S0009-2541(99)00106-0.
Roman, A., Arndt, N., 2020. Differentiated Archean oceanic crust: Its thermal structure, mechanical stability and a test of the sagduction hypothesis. Geochim. Cosmochim. Acta 278, 65–77. https://doi.org/10.1016/j.gca.2019.07.009.
Rustioni, G., Audetat, A., Keppler, H., 2021. The composition of subduction zone fluids and the origin of the trace element enrichment in arc magmas. Contributions to Mineralogy and Petrology 176 (7), 51. https://doi.org/10.1007/s00410-021-01810-8.
Rzehak, L.J.A., Kommescher, S., Kurzweil, F., Sprung, P., Leitzke, F.P., Fonseca, R.O.C., 2021. The redox dependence of titanium isotope fractionation in synthetic Ti-rich lunar melts. Contributions to Mineralogy and Petrology 176 (3), 19. https://doi.org/10.1007/s00410-020-01769-y.
Schmidt, M.W., Vielzeuf, D., Auzanneau, E., 2004. Melting and dissolution of subducting crust at high pressures: The key role of white mica. Earth. Planet. Sci. Lett. 228 (1), 65–84. https://doi.org/10.1016/j.epsl.2004.09.020.
Seixas, L.A.R., Bardintzeff, J.M., Stevenson, R., Bonin, B., 2013. Petrology of the high-Mg tonalites and dioritic enclaves of the ca. 2130Ma Alto Maranhão suite: Evidence for a major juvenile crustal addition event during the Rhyacian orogenesis, Mineiro Belt, southeast Brazil. Precambrian. Res. 238, 18–41. https://doi.org/10.1016/j.precamres.2013.09.015.
Sen, C., Dunn, T., 1994. Dehydration melting of a basaltic composition amphibolite at 1.5 and 2.0 GPa: Implications for the origin of adakites. Contributions to Mineralogy and Petrology 117 (4), 394–409. https://doi.org/10.1007/BF00307273.
Shirey, S.B., Hanson, G.N., 1984. Mantle-derived Archaean monzodiorites and trachyandesites. Nature 310 (5974), 5974. https://doi.org/10.1038/310222a0. Article.
Sisson, T.W., Kelemen, P.B., 2018. Near-solidus melts of MORB + 4 wt% H2O at 0.8–2.8 GPa applied to issues of subduction magmatism and continent formation. Contributions to Mineralogy and Petrology 173 (9), 70. https://doi.org/10.1007/s00410-018-1494-x.
Sizova, E., Gerya, T., Stüwe, K., Brown, M., 2015. Generation of felsic crust in the Archean: A geodynamic modeling perspective. Precambrian. Res. 271, 198–224. https://doi.org/10.1016/j.precamres.2015.10.005.
Skjerlie, K.P., Patiño Douce, A.E., 2002. The Fluid-absent Partial Melting of a Zoisite-bearing Quartz Eclogite from 1·0 to 3·2 GPa; Implications for Melting in Thickened Continental Crust and for Subduction-zone Processes. Journal of Petrology 43 (2), 291–314. https://doi.org/10.1093/petrology/43.2.291.
Smithies, R.H., Champion, D.C., 2000. The Archaean High-Mg Diorite Suite: Links to Tonalite–Trondhjemite–Granodiorite Magmatism and Implications for Early Archaean Crustal Growth. Journal of Petrology 41 (12), 1653–1671. https://doi.org/10.1093/petrology/41.12.1653.
Smithies, R.H., Champion, D.C., Sun, S.S., 2004. Evidence for Early LREE-enriched Mantle Source Regions: Diverse Magmas from the c. 3·0 Ga Mallina Basin, Pilbara Craton, NW Australia. Journal of Petrology 45 (8), 1515–1537. https://doi.org/10.1093/petrology/egh014.
Smithies, R.H., Lowrey, J.R., Sapkota, J., De Paoli, M.C., Hayman, P., Barnes, S.J., Champion, D.C., Masurel, Q., Thébaud, N., Grech, L.L., Drummond, M., Maas, R., 2022. Geochemical Characterisation of the Magmatic Stratigraphy of the Kalgoorlie and Black Flag Groups—Ora Banda to Kambalda region (No. 226). Department of Mines, Industry Regulation and Safety, Government of Western Australia.
Smithies, R.H., Lu, Y., Johnson, T.E., Kirkland, C.L., Cassidy, K.F., Champion, D.C., Mole, D.R., Zibra, I., Gessner, K., Sapkota, J., De Paoli, M.C., Poujol, M., 2019. No evidence for high-pressure melting of Earth's crust in the Archean. Nat. Commun. 10 (1), 5559. https://doi.org/10.1038/s41467-019-13547-x.
Smithies, R.H., Lu, Y., Kirkland, C., Cassidy, K., Champion, D., Sapkota, J., De Paoli, M., Burley, L., 2018. A New Look At Lamprophyres and sanukitoids, and Their Relationship to the Black Flag Group and Gold Prospectivity.
Smithies, R.H., Lu, Y., Kirkland, C.L., Johnson, T.E., Mole, D.R., Champion, D.C., Martin, L., Jeon, H., Wingate, M.T.D., Johnson, S.P., 2021. Oxygen isotopes trace the origins of Earth's earliest continental crust. Nature 592 (7852), 70–75. https://doi.org/10.1038/s41586-021-03337-1.
Spandler, C., Yaxley, G., Green, D.H., Rosenthal, A., 2008. Phase Relations and Melting of Anhydrous K-bearing Eclogite from 1200 to 1600°C and 3 to 5 GPa. Journal of Petrology 49 (4), 771–795. https://doi.org/10.1093/petrology/egm039.
Spencer, L.M., Albert, C., Williams, H.M., Nebel, O., Parkinson, I.J., Smithies, R.H., Bruno, H., Fowler, M., Moreira, H., Lissenberg, C.J., Millet, M.A., 2024. Titanium Stable Isotope and Major and Trace Element Compositions of Archean and Paleoproterozoic sanukitoids and Paleozoic high Ba-Sr granite Suites (Version 1). GFZ Data Services. https://doi.org/10.5880/digis.2024.004. Dataset.
Steenfelt, A., Garde, A.A., Moyen, J.F., 2005. Mantle wedge involvement in the petrogenesis of Archaean grey gneisses in West Greenland. Lithos. 79 (1), 207–228. https://doi.org/10.1016/j.lithos.2004.04.054.
Stern, R.A., Hanson, G.N., Shirey, S.B., 1989. Petrogenesis of mantle-derived, LILE-enriched Archean monzodiorites and trachyandesites (sanukitoids) in southwestern Superior Province. Can. J. Earth. Sci. 26 (9), 1688–1712. https://doi.org/10.1139/e89-145.
Syracuse, E.M., van Keken, P.E., Abers, G.A., 2010. The global range of subduction zone thermal models. Physics of the Earth and Planetary Interiors 183 (1), 73–90. https://doi.org/10.1016/j.pepi.2010.02.004.
Tamblyn, R., Hermann, J., Hasterok, D., Sossi, P., Pettke, T., Chatterjee, S., 2023. Hydrated komatiites as a source of water for TTG formation in the Archean. Earth. Planet. Sci. Lett. 603, 117982. https://doi.org/10.1016/j.epsl.2022.117982.
Till, C.B., Grove, T.L., Withers, A.C., 2012. The beginnings of hydrous mantle wedge melting. Contributions to Mineralogy and Petrology 163 (4), 669–688. https://doi.org/10.1007/s00410-011-0692-6.
van Hunen, J., Moyen, J.F., 2012. Archean Subduction: Fact or Fiction? Annu Rev. Earth. Planet. Sci. 40 (1), 195–219. https://doi.org/10.1146/annurev-earth-042711-105255.
van Hunen, J., van den Berg, A.P, 2008. Plate tectonics on the early Earth: Limitations imposed by strength and buoyancy of subducted lithosphere. Lithos. 103 (1), 217–235. https://doi.org/10.1016/j.lithos.2007.09.016.
Vandenburg, E.D., Nebel, O., Smithies, R.H., Capitanio, F.A., Miller, L., Cawood, P.A., Millet, M.A., Bruand, E., Moyen, J.F., Wang, X., Nebel-Jacobsen, Y., 2023. Spatial and temporal control of Archean tectonomagmatic regimes. Earth. Sci. Rev. 241, 104417. https://doi.org/10.1016/j.earscirev.2023.104417.
Wang, W., Huang, S., Huang, F., Zhao, X., Wu, Z., 2020. Equilibrium inter-mineral titanium isotope fractionation: Implication for high-temperature titanium isotope geochemistry. Geochim. Cosmochim. Acta 269, 540–553. https://doi.org/10.1016/j.gca.2019.11.008.
Wolf, M.B., Wyllie, P.J., 1994. Dehydration-melting of amphibolite at 10 kbar: The effects of temperature and time. Contributions to Mineralogy and Petrology 115 (4), 369–383. https://doi.org/10.1007/BF00320972.
Yaxley, G., Green, D., 1998. Reactions between eclogite and peridotite: Mantle refertilisation by subduction of oceanic crust. Schweizerische Mineralogische Und Petrographische Mitteilungen 78, 243–255.
Yogodzinski, G.M., Kelemen, P.B., Hoernle, K., Brown, S.T., Bindeman, I., Vervoort, J.D., Sims, K.W.W., Portnyagin, M., Werner, R., 2017. Sr and O isotopes in western Aleutian seafloor lavas: Implications for the source of fluids and trace element character of arc volcanic rocks. Earth. Planet. Sci. Lett. 475, 169–180. https://doi.org/10.1016/j.epsl.2017.07.007.
Young, E.D., Manning, C.E., Schauble, E.A., Shahar, A., Macris, C.A., Lazar, C., Jordan, M., 2015. High-temperature equilibrium isotope fractionation of non-traditional stable isotopes: Experiments, theory, and applications. Chemical Geology 395, 176–195. https://doi.org/10.1016/j.chemgeo.2014.12.013.
Zhang, C., Holtz, F., Koepke, J., Wolff, P.E., Ma, C., Bédard, J.H., 2013. Constraints from experimental melting of amphibolite on the depth of formation of garnet-rich restites, and implications for models of Early Archean crustal growth. Precambrian. Res. 231, 206–217. https://doi.org/10.1016/j.precamres.2013.03.004.

Zhang, J., Dauphas, N., M Davis, A., Pourmand, A, 2011. A new method for MC-ICPMS measurement of titanium isotopic composition: Identification of correlated isotope anomalies in meteorites. J. Anal. At. Spectrom. 26 (11), 2197–2205. https://doi.org/10.1039/C1JA10181A.

Zhang, Z.J., Dauphas, N., Johnson, A.C., Aarons, S.M., Bennett, V.C., Nutman, A.P., MacLennan, S., Schoene, B., 2023. Titanium and iron isotopic records of granitoid crust production in diverse Archean cratons. Earth. Planet. Sci. Lett. 620, 118342. https://doi.org/10.1016/j.epsl.2023.118342.

Zhao, X., Tang, S., Li, J., Wang, H., Helz, R., Marsh, B., Zhu, X., Zhang, H., 2020. Titanium isotopic fractionation during magmatic differentiation. Contributions to Mineralogy and Petrology 175 (7), 67. https://doi.org/10.1007/s00410-020-01704-1.